

Chapter 6

Doping Effect on Melting Temperature for Gold–Copper Bimetallic Nanocluster and Dependency on Bulk Melting Temperature to the Potential Model

Farid Taherkhani

Abstract Molecular dynamics (MD) simulation has been done for the melting temperature of gold–copper bimetallic nanostructure with 55 total gold and copper atom numbers and its bulk alloy. The trend of melting temperature for gold–copper bimetallic nanocluster is not the same as the melting temperature for gold–copper bulk alloy. MD simulation shows that the melting temperature of gold–copper bimetallic nanocluster increases with copper atom fraction. Semi-empirical potential within the tight-binding second moment approximation as new application potential model regarding the melting temperature for gold–copper bulk structure shows better result in comparison with EAM, Sutton–Chen potential and quantum Sutton–Chen potential models.

Keywords Molecular dynamics · Quantum Sutton–Chen potential · Semi-empirical potential · Gold–copper bimetallic nanostructure

6.1 Introduction

Nanoclusters are aggregates of atoms or molecules of nanometric size, containing a number of constituent particles ranging from 10 to 10^6 [1]. There are unusual chemical and physical properties in metallic nanocluster in comparison with metal bulk properties. Due to the extended applications of metallic nanoclusters in heterogeneous catalysts, electronic devices and microelectronics, investigation of their structural and dynamical properties are topics of interest in previous literature

This chapter book is dedicated to my parents due to their endless support and encouragement

F. Taherkhani (✉)

School of Nano-Science, Institute for Research in Fundamental Sciences (IPM), 19395-5531 Tehran, Iran
e-mail: faridtaherkhani@gmail.com

[2, 3]. Applications of metal nanoclusters to heterogeneous catalysis have shown that good selectivity can be achieved toward specific reactions by controlling the catalyst surface composition [4]. Gold nanoparticle catalysts are used mainly in selective oxidation reactions and in a broad range of organic transformations besides hydrogenation [5]. Copper nanoparticles are known to be active in the oxidation of alcohols to aldehydes [6]. Therefore, by mixing the two metals, Au–Cu bimetallic nanoclusters offer a way to fine-tune the catalytic properties of these two metals. Nevertheless, understanding their structural–thermal stability relationship is a difficult task.

Molecular dynamics (MD) simulation is an ideal tool for investigating the thermal physical properties of such small clusters. Among different bimetallic alloy nanoparticle catalysts, Au–Cu catalysts have recently attracted interest for catalytic oxidation of CO, benzyl alcohol, and propene [7–9] and for the partial oxidation of methanol to produce hydrogen fuels. Some recent experimental results indicate that the icosahedral phase structure can be stabilized with the addition of some transition or noble metal to a pure metallic cluster [10]. It is known that for pure 55-atom coinage clusters, only the Ag₅₅ and Cu₅₅ exhibit the icosahedral structure, whereas the Au₅₅ cluster has a low-symmetry C_1 structure [11–13]. Gao and co-workers recently studied doping a single metal atom to the Au₅₅ cluster. They found that a single-atom dopant is unlikely to convert the low-symmetry parent structure to the icosahedral (I_h) structure [14]. It is found that doping of Au₅₅ with a single Cu atom can sharply raise the melting point of the cluster. It is well known that the melting temperature of Au₅₅ (380 K) is much lower than that of Cu₁Au₅₄ (530 K) [15]. A Cu–Au cluster does not experience a smooth transition from a pure Cu-like behavior to a pure Au cluster with a decrease in the concentration of Cu. The thermal behavior of Cu–Au is mainly influenced by the presence of Cu atoms in the bimetallic structure [16]. Studies of phase conformations and thermal behavior of Au–Cu binary clusters by classical MD simulations showed that the cluster size, the concentration in the alloy, and the annealing temperature have a dominant effect on the morphology reconstruction process [17]. For example, when the starting morphology is of a cuboctahedral type, by changing the concentration of copper from 50 to 10 %, an optimum stability of an icosahedral-type morphology is found at a bimetallic concentration of gold 75 % and copper 25 %, in fair agreement with experimental reports [18]. In the small size of nanostructure, as the surface-to-volume ratio is large, the surface effect has a significant contribution on physical quantities such as transport properties, melting point, and thermal energy [19, 20]. One of the most commonly used parameters for the description of the energetic situation on the surface of a solid is the surface energy. The surface energy may be defined as the excess energy of the surface of a material compared to its bulk. Joseph and co-workers have investigated the relative surface energy changes with temperature for two bimetallic alloys. At low temperatures, they found the segregation to be dependent primarily on the surface energy difference for Pt–Pd and Cu–Ni systems. In the Pt–Pd system, the surface energy difference between pure Pt and Pd increases with an increase of temperature. This behavior was different from that of a Cu–Ni bimetallic alloy where the surface energy

difference decreases with an increase of temperature [15]. Knowledge of diffusion behavior is of interest for the production of metallic materials and for their practical use in the near phase transition. On this basis, investigations were performed on the Pt–Pd [15], Cu–Ni [19], Ag–Pt [21], Au–Pd [22], and Fe–Al [23] systems. In all cases, self-diffusion coefficient was found to increase with temperature. Self-diffusion coefficient decreases with pressure [24–26]. Near the melting temperature, the spin multiplicity of bimetallic nanocluster changes in comparison with its solid state completely [25, 26]. In the present study, we show that the presence of impurity at the pure cluster affects the melting temperature for gold–copper bimetallic nanostructure as well as the bulk structure. In this work, we study the structure details and dynamic behavior of Au–Cu nanoclusters for the specific case of icosahedral geometry and the variation of the configurational energy with temperature.

6.2 MD Simulation Details

In classical MD, each particle is treated as a point mass and the motion is governed by Newton’s second law. The thermodynamic properties are obtained from time averages over the ensembles of particles.

MD simulations were done in the constant temperature ensemble (NVT) using the Verlet algorithm for the integration of Newton’s equations of motion, with a time step of one femto second resulting in long simulation runs of 500 picoseconds (ps). Ensemble averaging has been done after 400 ps. The Nose–Hoover thermostat is used for controlling the temperature of MD simulation with DL POLY package [27]. The quantum Sutton–Chen (QSC) many-body inter-atomic potential leads to an accurate description of many properties of I_h metals and their alloys. In this work, we have applied the QSC inter-atomic potential to model the interaction in the Au–Cu alloy clusters. A cut-off ratio for the range of the interaction of 7.0 Å was used in all the cases.

6.3 Potential Function

MD simulations using DL POLY were used to gain insights into the melting process at the atomistic level. All the thermodynamic and transport properties were obtained as time averages over the particle positions and velocities. The local electronic density is included to account for the many-body terms [15]. Based on the Sutton–Chen potential, the potential energy of the finite system is given by

$$U_{\text{tot}} = \sum_i U_i = \sum_i \varepsilon \left[\sum_{j \neq i} \frac{1}{2} V(r_{ij}) - c \rho_i^{1/2} \right] \quad (6.1)$$

where r_{ij} is the distance between atoms i and j , c a positive dimensionless parameter and ε a parameter with the dimensions of energy. Parameter $V(r_{ij})$ is a pair potential for including the repulsion of Pauli's exclusion principle:

$$V(r_{ij}) = \left(\frac{a}{r_{ij}}\right)^n \quad (6.2)$$

The local density ρ_i accounting for cohesion associated with any atom i is given by

$$\rho_i = \sum_{j \neq i} \phi(r_{ij}) = \sum_{j \neq i} \left(\frac{a}{r_{ij}}\right)^m \quad (6.3)$$

where a is a length parameter scaling all spacing (leading to dimensionless V and ρ); n and m are both positive integer parameters with condition $n > m$.

Sutton and Chen restricted values of m to be greater than 6 and fitted it to give close agreement with the bulk modulus and the elastic constants. The Sutton–Chen potential predicts properties involving defects, surfaces, and interfaces poorly. The quantum Sutton–Chen potential includes quantum corrections and takes into account the zero-point energy allowing better prediction of temperature-dependent properties. The QSC potential function was found to be better suited to melting and phase transformation studies of bulk Cu–Ni [28], Cu–Au [29], and Pd–Ni [30] alloys. The QSC parameters for Au and Cu are listed in Table 6.1 [29].

Semi-empirical potential derived within the tight-binding second moment approximation as in Eq. 6.4 by Cleri and Rosato was applied to describe interactions for bulk systems.

$$E = \sum_j E_j^b - E_j^r \quad (6.4)$$

where E_j^b, E_j^r are bonding and repulsion of Born–Mayer term and can be written as Eqs. 6.5 and 6.6, respectively.

$$E_j^b = \sqrt{\sum_i \xi_{sw}^2 e^{\left[-2q_{sw} \left(\frac{r_{ji}}{r_{sw}^0} - 1\right)\right]}} \quad (6.5)$$

$$E_j^r = \sum_i A_{sw} e^{\left[-p_{sw} \left(\frac{r_{ji}}{r_{sw}^0} - 1\right)\right]} \quad (6.6)$$

Table 6.1 QSC potential parameters for Au and Cu

Metal	n	m	ε (eV)	C	a (Å)
Au	11	8	1.27940E-2	34.4280	4.07830
Cu	10	5	1.23860E-2	39.7550	3.61530

Table 6.2 Gupta potential parameters for Au and Cu

Parameter	Cu–Cu	Au–Cu	Au–Au
A/eV	0.0855	0.1539	0.2061
p	10.960	11.050	10.229
$r_o/\text{Å}$	2.556	2.556	2.884
ξ/eV	1.2240	1.5605	1.7900
q	2.2780	3.0475	4.0360

r_{ji} is the distance between the atoms at sites, i.e., j ; $s = A, B$ is the chemical species of the atom j , while $w = A, B$ is the species of the atom i , r_{sw}^0 is the nearest-neighbors distance. The parameters A_{sw} , p_{sw} , q_{sw} , ξ_{sw} are fitted to several bulk properties of the $\text{Au}_{0.25}\text{Cu}_{0.75}$ cubic alloy. The parameters of mentioned empirical potential can be defined with the exact work of Cleri and Rosato [31] which is presented at Table 6.2.

6.4 Results and Discussion

6.4.1 Solid–Liquid Phase Transition in Bulk Au–Cu Alloy

The effects of impurity on the melting point of $\text{Cu}_x\text{Au}_{55-x}$ are investigated. Sutton–Chen (SC) [32], quantum Sutton–Chen (Q-SC) many-body [32] and embedded atom method (EAM) [33] potentials are used. For comparison of the different potential models we have chosen semi-empirical potential models for investigation of the melting temperature of copper–gold alloy in bulk structure. Many techniques such as distortion parameter [34–37], thermal conductivity [19, 20], self-diffusion coefficient [38, 39], heat capacity [18, 40, 41], phase-field-crystal models [42], local pressure tensor [43] and Lindemann index [44] can be used for recognition of solid–liquid phase transition [34].

On the basis of Fig. 6.1, the structural configuration at 300 K for 0.250 mol fraction of gold in copper is more stable than other doping fractions such as 0.75 and 0.50 mol fraction of copper in gold due to more interaction between gold and copper atoms. Chemical ordering effect is investigated on the phase transition of solid–liquid bimetallic nanocluster. Heat capacity is used for investigation of solid–liquid phase of gold–copper alloy transition as well. The results of melting temperature with Gupta potential model are represented in Table 6.3. According to Table 6.3 the following order for melting temperature is observed:

$$\text{Cu} > \text{Au} > \text{Cu}_{0.75}\text{Au}_{0.25} > \text{Cu}_{0.25}\text{Au}_{0.75} > \text{Cu}_{0.5}\text{Au}_{0.5}$$

On the basis of Table 6.3, the bulk melting temperature with Gupta potential model shows good agreement with available experimental data in comparison with other potential models such as quantum Sutton–Chen, EAM and Sutton–Chen. The

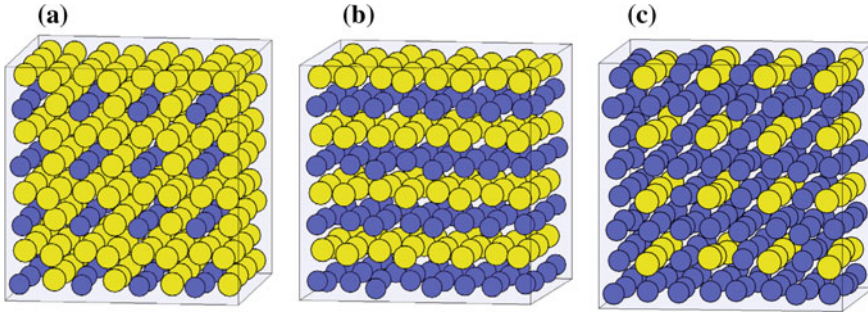


Fig. 6.1 Optimum structure for copper–gold alloy **a** 0.25 copper mole fraction in gold; **b** 0.50 copper mole fraction in gold; **c** 0.75 copper mole fraction in gold

Table 6.3 Melting points obtained from MD simulations with Gupta potential model for bulk Au–Cu and comparison potential model with experiments

Composition	T_m^{EAM}	T_m^{SC}	T_m^{QSC}	T_m^{Gupta}	T_m^{EXP}
Cu	1320.5 ± 1.5	1150 ± 10	1370 ± 10	1338 ± 2	1356
Au	1182.5 ± 1.5	1120 ± 10	1420 ± 10	1325 ± 2	1336
AuCu ₃	1240.5 ± 1.5	1110 ± 10	1340 ± 10	1225 ± 2	1250
AuCu	1173.5 ± 0.5	–	1360 ± 10	1200 ± 2	1185
Au ₃ Cu	1151.5 ± 1.5	1020 ± 20	1370 ± 10	1220 ± 2	1220

results of heat capacity for investigation of solid–liquid phase transition of pure bulk gold and copper are given in Fig. 6.2. There is a peak in the heat capacity graph, which is proportional to the melting temperature for pure and gold bulk structure.

On the basis of Fig. 6.2, our results for copper and gold in bulk, solid–liquid phase transition are 1338 and 1325 K, respectively, and are consistent with the corresponding experimental results of 1356 and 1337 K.

6.4.2 Solid–Liquid Phase Transition in Bimetallic Nanocluster Au–Cu

MD simulation has been used for studying the melting temperature of bimetallic Au–Cu system with total atom 55. The most direct way to analyze the thermal behavior is to consider the configuration energy versus temperature. For this purpose, we calculated the configuration energy at different temperatures; the melting temperature (T_m) of the system would be located at the point where the thermal

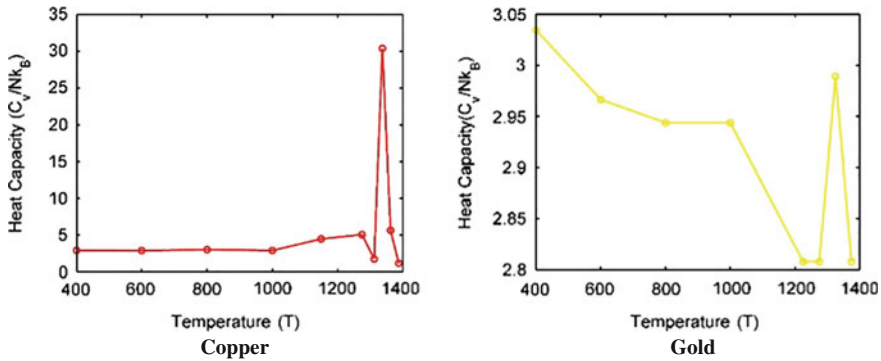


Fig. 6.2 Heat capacity for copper and gold bulk structure versus temperature

behavior line presents a change in the slope. On the basis of configuration energy, the slope is not sharp and seems relatively wide. We observe that the configuration energy shows a simple jump as a function of temperature at the melting point of the solid. The results of configuration energy for different chemical compositions namely $\text{Cu}_6\text{Au}_{49}$, $\text{Cu}_{12}\text{Au}_{43}$, $\text{Cu}_{18}\text{Au}_{37}$, $\text{Cu}_{27}\text{Au}_{28}$, $\text{Cu}_{41}\text{Au}_{14}$, and $\text{Cu}_{49}\text{Au}_6$ gold–copper bimetallic nanoclusters are presented in Fig. 6.3.

The melting point of bimetallic Au–Cu 55 atom nanoclusters is examined using the quantum Sutton–Chen many-body potential function. The impurity effect on the melting point for $\text{Cu}_6\text{Au}_{49}$, $\text{Cu}_{12}\text{Au}_{43}$, $\text{Cu}_{18}\text{Au}_{37}$, $\text{Cu}_{41}\text{Au}_{14}$, $\text{Cu}_{49}\text{Au}_6$ and Cu_{55} bimetallic nanoclusters is considered. The results of melting temperature as a function of doping are presented in Fig. 6.4.

According to Fig. 6.4, the melting temperature of gold–copper bimetallic nanocluster increases with copper atom fraction. The trend of melting temperature for bulk gold–copper is not the same as the melting temperature trend for gold–copper bimetallic nanocluster. The surface energy effect is an important phenomenon which is observed in nanosystem but not in bulk structure [40, 41]. Previous literature shows that the surface energy of gold nanoparticle is less than that of copper nanoparticle [40, 41]. As a result, most of the gold atoms move on the surface. The strength of metallic bond for copper is greater than that of gold, thus the melting temperature of gold–copper bimetallic nanocluster increases with higher copper atom fraction due to surface effect. The melting temperature of bimetallic gold–copper nanoclusters has been calculated by Cheng et al. [14]. The results indicate that the melting temperature of Au_{55} increases with doping of copper as impurity. Canonical Monte Carlo simulations [14], based on the second-moment approximation of the tight-binding potentials, are consistent with our results. On the basis of Fig. 6.4, the melting temperature for gold–copper bimetallic nanoclusters is lower than the melting temperature of bulk structure significantly.

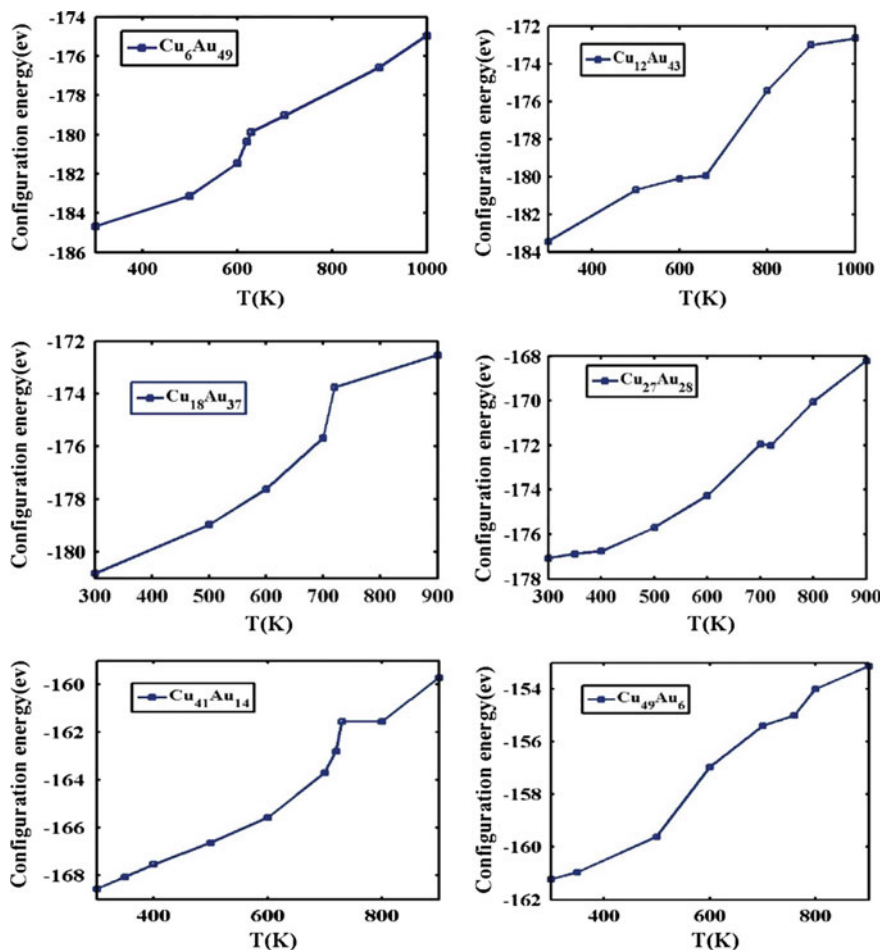
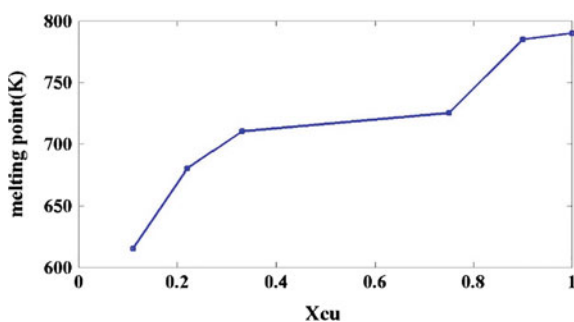


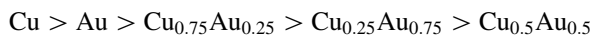
Fig. 6.3 Configurational energy versus temperature for $\text{Cu}_6\text{Au}_{49}$, $\text{Cu}_{12}\text{Au}_{43}$, $\text{Cu}_{18}\text{Au}_{37}$, $\text{Cu}_{27}\text{Au}_{28}$, $\text{Cu}_{41}\text{Au}_{14}$ and $\text{Cu}_{49}\text{Au}_6$ bimetallic nanoclusters

Fig. 6.4 Melting temperature versus copper atom fraction in gold-copper bimetallic nanocluster



6.5 Conclusions

Configurational energy analysis has been used for the determination of melting temperature of gold–copper bimetallic nanoclusters. MD simulation with semi-empirical potential within the tight-binding second moment approximation has been used as a new application potential model for the melting temperature of gold–copper bulk structure. Optimum structure of gold–copper bulk structure has been obtained with MD simulation as well. The following order for the melting temperature of gold–copper alloy in bulk structure was observed:



Semi-empirical potential model for the melting temperature shows good agreement with available experimental data in comparison with EAM, quantum Sutton–Chen and Sutton–Chen potential models. MD simulation regarding the melting temperature of gold–copper bimetallic nanoclusters with a total of 55 atoms shows that the melting temperature increases with copper atom fraction due to lower surface energy and metallic bond energy of gold. MD simulation with Quantum Sutton–Chen potential model estimates the melting temperature of gold–copper bimetallic nanoclusters around 600–800 K temperature range which is significantly lower than its bulk structure.

References

1. Baletto F, Ferrando R (2005) Structural properties of nanoclusters: energetic, thermodynamic, and kinetic effects. *Rev Mod Phys* 77:371–423
2. Ferrando R, Jellinek J, Johnston RL (2008) Nanoalloys: from theory to applications of alloy clusters and nanoparticles. *Chem Rev* 108:845–910
3. Huang S-P, Mainardi DS, Balbuena PB (2003) Structure and dynamics of graphite-supported bimetallic nanoclusters. *Surf Sci* 545:163–179
4. Bracey CL, Ellis PR, Hutchings GJ (2009) Application of copper–gold alloys in catalysis: current status and future perspectives. *Chem Soc Rev* 38:2231–2243
5. Della Pina C, Falletta E, Prati L, Rossi M (2008) Selective oxidation using gold. *Chem Soc Rev* 37:2077–2095
6. Yoo W-J, Li C-J (2007) Copper-catalyzed oxidative esterification of alcohols with aldehydes activated by Lewis acids. *Tetrahedron Lett* 48:1033–1035
7. Liu X, Wang A, Wang X, Mou C-Y, Zhang T (2008) Au–Cu alloy nanoparticles confined in SBA-15 as a highly efficient catalyst for CO oxidation. *Chem Commun* 27:3187–3189
8. Zhang L (2012) A molecular dynamics study of thermal behavior of melting an Au₅₄Cu₁ cluster. *Procedia Eng* 36:207–211
9. Zhang L, Zhang C-B, Qi Y (2008) Local structure changes of 54-, 55-, 56-atom copper clusters on heating. *Phys Lett A* 372:2874–2880
10. Huang W, Ji M, Dong C-D, Gu X, Wang L-M, Gong XG, Wang L-S (2008) Relativistic effects and the unique low-symmetry structures of gold nanoclusters. *ACS Nano* 2:897–904
11. Gao Y, Shao N, Pei Y, Zeng XC (2010) Icosahedral crown gold nanocluster Au₄₃Cu₁₂ with high catalytic activity. *Nano Lett* 10:1055–1062

12. Häkkinen H, Moseler M, Kostko O, Morgner N, Hoffmann MA, Issendorff BV (2004) Symmetry and electronic structure of noble-metal nanoparticles and the role of relativity. *Phys Rev Lett* 93:093401
13. Xing X, Danell RM, Garzón IL, Michaelian K, Blom MN, Burns MM, Parks JH (2005) Size-dependent fivefold and icosahedral symmetry in silver clusters. *Phys Rev B* 72:081405
14. Cheng D, Huang S, Wang W (2006) Thermal behavior of core-shell and three-shell layered clusters: melting of $\text{Cu}_1\text{Au}_{54}$ and $\text{Cu}_{12}\text{Au}_{43}$. *Phys Rev B* 74:064117
15. Sankaranarayanan SK, Bhethanabotla VR, Joseph B (2005) Molecular dynamics simulation study of the melting of Pd–Pt nanoclusters. *Phys Rev B* 71:195415
16. Rodríguez-López J, Montejano-Carrizales J, José-Yacamán M (2003) Molecular dynamics study of bimetallic nanoparticles: the case of Au_xCu_y alloy clusters. *Appl Surf Sci* 219:56–63
17. Yin J, Shan S, Yang L, Mott D, Malis O, Petkov V, Cai F, Shan Ng M, Luo J, Chen BH (2012) Gold–copper nanoparticles: nanostructural evolution and bifunctional catalytic sites. *Chem Mater* 24:4662–4674
18. Taherkhani F, Akbarzadeh H, Abroshan H, Fortunelli A (2012) Dependence of self-diffusion coefficient, surface energy, on size, temperature, and Debye temperature on size for aluminum nanoclusters. *Fluid Phase Equilib* 335:26–31
19. Huang S-P, Balbuena PB (2002) Melting of bimetallic Cu–Ni nanoclusters. *J Phys Chem B* 106:7225–7236
20. Taherkhani F, Rezaia H (2012) Temperature and size dependency of thermal conductivity of aluminum nanocluster. *J Nanopart Res* 14:1–8
21. Negreiros F, Taherkhani F, Parsafar G, Fortunelli A (2012) Kinetics of chemical ordering in a Ag–Pt nanoalloy particle via first-principles simulations. *J Chem Phys* 137:194302
22. Mejía-Rosales SJ, Fernández-Navarro C, Pérez-Tijerina E, Montejano-Carrizales JM, José-Yacamán M (2006) Two-stage melting of Au–Pd nanoparticles. *J Phys Chem B* 110:12884–12889
23. Mehrer H, Eggersmann M, Gude A, Salamon M, Sepiol B (1997) Diffusion in intermetallic phases of the Fe–Al and Fe–Si systems. *Mater Sci Eng A* 239:889–898
24. Holzapfel C, Chakraborty S, Rubie D, Frost D (2009) Fe–Mg interdiffusion in wadsleyite: the role of pressure, temperature and composition and the magnitude of jump in diffusion rates at the 410 km discontinuity. *Phys Earth Planet Inter* 172:28–33
25. Lott K, Nirk T, Volobujeva O (2002) Chemical self-diffusion in undoped ZnS and in undoped CdSe. *Cryst Eng* 5:147–153
26. Palagin D, Doye PK (2014) Ni-based nanoalloys: towards thermally stable highly magnetic materials. *J Chem Phys* 141:214302
27. Smith W, Todorov IT (2006) A short description of DL_POLY. *Mol Simul* 32:935–943
28. Qi Y, Çağın T, Kimura Y, Goddard WA III (1999) Molecular-dynamics simulations of glass formation and crystallization in binary liquid metals: Cu–Ag and Cu–Ni. *Phys Rev B* 59:3527–3533
29. Qi Y, Çağın T, Kimura Y, Goddard WA III (2001) Viscosities of liquid metal alloys from non-equilibrium molecular dynamics. *J Comput Aided Mater* 8:233–243
30. Özdemir KS, Tomak M, Uludoğan M, Çağın T (2004) Liquid properties of Pd–Ni alloys. *J Non-Cryst Solids* 337:101–108
31. Cleri F, Rosato V (1993) Tight-binding potentials for transition metals and alloys. *Phys Rev B* 48:22
32. Kart H, Tomak M, Çağın T (2005) Thermal and mechanical properties of Cu–Au intermetallic alloys. *Model Simul Mater Sci* 13:657–669
33. Lv YJ, Chen M (2011) Thermophysical properties of undercooled alloys: an overview of the molecular simulation approaches. *Int J Mol Sci* 12:278–316
34. Akbarzadeh H, Yaghoubi H, Shamkhali AN, Taherkhani F (2013) Effects of gas adsorption on the graphite-supported Ag nanoclusters: a molecular dynamics study. *J Phys Chem C* 117:26287–26294

35. Akbarzadeh H, Yaghoubi H, Shamkhali AN, Taherkhani F (2014) CO adsorption on Ag nanoclusters supported on carbon nanotube: a molecular dynamics study. *J Phys Chem C* 118:9187–9195
36. Taherkhani F, Freshteh Seresh P (2015) Doping effect on the Janus-like structure of a copper–iron bimetallic nanocluster and its solid–liquid phase transition. *PTEP* 4:043I01, 1–12
37. Taherkhani F, Parviz Z, Akbarzadeh H, Fortunelli A (2015) Temperature and doping effect on thermal conductivity of copper–gold icosahedral bimetallic nanoclusters and bulk structures. *J Phys Chem C* 119:7922–7932
38. Ala-Nissila T, Ferrando R, Ying S (2002) Collective and single particle diffusion on surfaces. *Adv Phys* 51:949–1078
39. Taherkhani F, Negreiros FR, Parsafar G, Fortunelli A (2010) Simulation of vacancy diffusion in a silver nanocluster. *Chem Phys Lett* 498:312–316
40. Taherkhani F, Akbarzadeh H, Rezaia H (2014) Chemical ordering effect on melting temperature, surface energy of copper–gold bimetallic nanocluster. *J Alloy Compd* 617:746–750
41. Akbarzadeh H, Taherkhani F (2013) Cluster size dependence of surface energy of Ni nanocluster: a molecular dynamics study. *Chem Phys Lett* 558:57–61
42. Heinonen V, Achim CV, Elder KR, Buyukdagli S, Ala-Nissila T (2014) Phase-field-crystal models and mechanical equilibrium. *Phys Rev E* 89:032411
43. Laasonen K, Panizon E, Bochicchio D, Ferrando R (2013) Competition between icosahedral motifs in AgCu, AgNi, and AgCo nanoalloys: a combined atomistic–DFT study. *J Phys Chem C* 117:26405–26413
44. Alavi S, Thompson DL (2006) Molecular dynamics simulations of the melting of aluminum nanoparticles. *J Phys Chem A* 110:1518–1523